(article starts on next page)

Osteoarthritis and Cartilage

OARSI — OSTEOARTHRITIS RESEARCH SOCIETY INTERNATIONAL

Synovial fluid profile dictates nanoparticle uptake into cartilage - implications of the protein corona for novel arthritis treatments

U. von Mentzer †, T. Selldén †, L. Råberg †, G. Erensoy †, A.-K. Hultgård Ekwall ‡ §,
A. Stubelius † *

† Division of Chemical Biology, Department of Biology and Biological Engineering, Chalmers University of Technology, Gothenburg, Sweden
‡ The Rheumatology Clinic, Sahlgrenska University Hospital, Gothenburg, Sweden
§ Department of Rheumatology and Inflammation Research, Institute of Medicine, Sahlgrenska Academy, University of Gothenburg, Gothenburg, Sweden

SUMMARY

Objective: Drug delivery strategies for joint diseases need to overcome the negatively charged cartilage matrix. Previous studies have extensively investigated particle approaches to increase uptake efficiency by harnessing the anionic charge of the cartilage but have neglected to address interactions with the protein-rich biological environment of the joint space. We aimed to evaluate the effects of hard protein coronas derived from osteoarthritis (OA) and rheumatoid arthritis (RA) patient synovial fluids as well as the commonly used fetal calf serum (FCS) on nanoparticle (NP) uptake into tissues and cells.
Methods: We developed a NP panel with varying PEGylation and incubated them with synovial fluid from either OA, RA patients or FCS. We evaluated the effects of the formed NP-biocorona complex uptake into the porcine articular cartilage explants, chondrocytes and monocyte cell lines and primary patient FLS cells. Proteins composing hard biocoronas were identified using a quantitative proteomics approach.
Results: Formed biocoronas majorly impacted NP uptake into cartilage tissue and dictated their uptake in chondrocytes and monocytes. The most suitable NP for potential OA applications was identified. A variety of proteins that were found on all NPs, irrespective of surface modifications. NP-, and protein-specific differences were also observed between the groups, and candidate proteins were identified that could account for the observed differences.
Conclusions: This study demonstrates the impact of protein coronas from OA and RA patient synovial fluids on NP uptake into cartilage, emphasizing the importance of biological microenvironment considerations for successful translation of drug delivery vehicles into clinics.

Introduction

A major obstacle for therapies targeting joint diseases has been to reach the chondrocytes deeply embedded in the extracellular cartilage matrix (ECM). This dense, avascular, and aneural network of structural and negatively charged macromolecules poses a physical barrier to reaching the cells, thus serving as a target for cartilage-associated diseases such as osteoarthritis (OA).

Recent intra-articular drug delivery systems have leveraged small nanosized particles and electrostatic interactions with the anionic ECM to achieve enhanced delivery efficiency, targeting, and solubility[1–3].

The therapeutic potential of nanoparticles (NPs) for arthritis also depends on their fate in the joint, where synovial space retention and escaping immune clearance are pivotal for increased tissue uptake[4]. Such outcomes, however, are determined by the distinct biological identity of the NPs arising from host-derived components and their interactions with the material[5]. These bioactive proteins, carbohydrates, and lipids alter particle size and surface composition, which dictate their physiological outcomes[5,6]. Studies on systemic administration have demonstrated that human subjects vary widely in their response to nanomedicine. A minor

* Address correspondence and reprint requests to: A. Stubelius, Kemivägen 10, 41296 Gothenburg, Sweden.
E-mail address: Alexandra.stubelius@chalmers.se (A. Stubelius).

change from blood plasma to serum profoundly influences the protein corona composition and the subsequent interplay between NPs and cells[7,8]. For arthritis, synovial fluid (SF) has indeed shown to influence diffusional transport of NPs, raising the need for further investigations into mechanisms of how we can achieve and develop specific nanotechnologies targeting joint-related diseases[9,10].

To address the issue of how the acquired biological identity could influence the delivery efficiency of NPs in the joint, we employed intrinsically cationic polyamidoamine (PAMAM) dendrimers as drug delivery systems. Due to their small size, surface functionality, and hydrophilicity, PAMAMs have been extensively characterized and investigated for their transport of various cargo including drugs[11], nucleic acids[12], growth factors[13], and interactions with serum proteins[14]. By modifying PAMAM's surface chemistries utilizing different lengths of polyethylene glycol (PEG), we designed a panel of small nanocarriers to study the impact of osteoarthritis (OA) and rheumatoid arthritis (RA) patient SFs as well as the commonly used fetal calf serum (FCS) on NP uptake into the cartilage and cells. This study is the first to demonstrate the implications of patient SF protein corona formation on small cationic nanocarriers, emphasizing the importance of using relevant biological microenvironments for successful advances in intra-articular drug delivery and translation into clinics.

Methods

Materials and reagents

The full list of materials and reagents can be found in the Supplementary material.

Material synthesis

PEGylation was performed using the methods of Geiger *et al.*[13] and Zhao *et al.*[15]. mPEG was activated using 4-NPC, dried, purified, dissolved in DMSO, and combined with PAMAM G5 solution (1.585 mM, $NaHCO_3$, pH $= 8$) at the stoichiometric ratio of 1:3 to achieve ~2% surface PEGylation and allowed to react for 24 h (stirring, room temperature; RT). The product was dialyzed, dried, and stored at $-20°C$ until further use.

Modified PAMAM compounds ($NP_0 = 0\%$ mPEG, $NP_{350} = 2\%$ $mPEG_{350}$, $NP_{5000} = 2\%$ $mPEG_{5000}$) were dissolved (5 mg/mL, PBS, pH $= 7.4$) and reacted with fluorescein isothiocyanate isomer I (FITC) in acetone (molar ratio 1:5, dark conditions, 12h, RT). The samples were dialyzed, freeze-dried, and set to the final concentration (c_{final}) of 30 μM in PBS (pH $= 7.4$).

Material characterization

The fluorescence signal (FITC, λ_{ex} 483/14 nm/λ_{em} 530/30 nm) was quantified using a CLARIOstar Plus (BMG Labtech, Offenburg, Germany) microplate reader. FITC-labeled NPs were dissolved in methanol, diluted with PBS ($c_{final} = 2$ μg/mL), and compared to a standard curve. Labeling efficiency was calculated as a proportion of FITC weight to the weight of modified FITC labeled NPs.

Transmission electron microscope (TEM) images were obtained by NPs (15 μM, pH 6, briefly sonicated) being placed on a 3 mm holey carbon film-coated copper grid (Ted Pella, Inc., Redding, California), stained with 4% sodium phosphotungstate, air-dried at RT, and imaged using FEI Tecnai T20 at 200 kV. NP size and zeta potential were assessed using the dynamic light scattering (DLS) Zetasizer Nano ZS system (Malvern Instruments, UK), where hydrodynamic diameters and zeta potentials are reported as means of three runs for each sample.

Biocompatibility of NPs was investigated in L929 (mouse fibroblast), Tc28a2 (human chondrocyte), and U937 (human monocyte) cell lines using a resazurin metabolic activity assay.

Protein corona isolation/formation

All patients have provided informed consent and the procedure was approved by the Ethics Committee of Gothenburg University (Ethical approval Dnr: 573-07). SF samples from 5 (4f/1m, 65–80 years old) RA patients and 4 (2f/2m, 45–82 years old) late OA patients were collected during aseptic aspiration of knee joints at the Rheumatology Clinic and Orthopaedic Clinic, respectively, at Sahlgrenska University Hospital, Gothenburg, Sweden.

Patient SF and control FCS samples were pooled according to the disease profile (5×10^8 particles or 2 μg), diluted 1:20 in PBS, and mixed with 30 μM NP solution (1:1, v/v). The samples were incubated at $37°C$ while shaking for 1 h at 100 rpm to resemble the dynamic environment of the SF in the joint and address the Vroman effect. To preserve the proteins bound with high affinity known as the hard protein coronas, NPs were spun down at $15,000 \times g$ for 15 min and washed three times with chilled PBS. Final concentration of NP-protein complexes was 1 μg/mL (2.5×10^8 particles/mL).

Protein content in the explant media was assessed using a Pierce BCA protein assay kit according to the manufacturer's instructions.

Biological interactions with NPs

Porcine cartilage tissues were obtained from the Experimental Biomedicine animal facilities under the 3R principle (Gothenburg, Sweden). Explants were extracted from the femoral and tibial condyle cartilage of the 3-6-month-old pigs using biopsy punchers ($d = 4$ mm) (Kai Medical, Honolulu, USA), trimmed (~2 mm) to exclude subchondral bone, and immediately frozen in PBS supplemented with 1 % 10,000 U/mL Penicillin, Streptomycin (Gibco) and protease inhibitors (Roche, Switzerland). Explants were thawed, weighed to ensure uniformity, and allowed to equilibrate overnight in DMEM supplemented with 25 mM HEPES. 100 μL of 30 μM NP-protein solutions were administered to the porcine explants and incubated for 4 or 24 h ($c_{final} = 12$ μM). NP uptake into cartilage was revealed by measuring the overall FITC fluorescence over time and comparing the initial supernatant signal pre-incubation T_{0h} (100 %) to reduced values after 4 (T_{4h}) or 24 (T_{24h}) hours. Each explant condition was performed in triplicates and repeated independently three times. To visualize NP uptake, 24 h cartilage explants were fixed in 2% paraformaldehyde, sliced in half, cut along the sagittal plane from the center, stained with DAPI, and imaged using Nikon Ti2 inverted microscope with a 20x objective. Images were obtained using ImageJ software.

Cellular uptake was investigated utilizing the Tc28a2 chondrocyte cell line (gift from Dr. Cronstein's lab at NYU Langone, USA), U937 monocyte cell line (Sigma—Aldrich), and RA (3f, 59–66 years old) or OA (2f/1m, 67–77 years old) patient-derived fibroblast-like synoviocytes (FLS) (Sahlgrenska University Hospital, Gothenburg, Sweden). The cells were seeded under serum-free conditions at the density of 1×10^5 cells/well in a 48-well plate, incubated with the NPs for 30 min or 10 h (cell lines included additional time points), and washed three times with FACS buffer. Quantification of cellular uptake was performed using Guava EasyCyte 8HT flow cytometer (Millipore, Darmstadt, Germany) by measuring the FITC signal (λ_{ex} 488 nm/λ_{em} 525/30 nm). Gating included only single, live cells (after FSC/SSC exclusion of dead cells, >5000 cells) with an acquisition range of 5000–10,000 cells. The mean cellular uptake of FITC-labeled NPs was estimated as the average fluorescence intensity of all cells within the gate. The data was collected in 1–3 independent experiments and is represented as the means with

95% confidence intervals (CI), $n = 3–4$. All flow cytometry data were analyzed and visualized using FlowJo software V10.

Proteomic analysis

NPs with hard protein coronas were pelleted by centrifugation at $15,000 \times g$ for 15 min, snap-frozen using liquid nitrogen, and submitted to the Proteomics Core Facility (Gothenburg, Sweden). Briefly, proteins were digested into peptides using MS-grade trypsin and analyzed by nanoscale liquid chromatography-tandem mass spectrometry LC-MS/MS. The mascot search engine was used to match the discovered peptide sequences against SwissProt human and bovine protein database using Proteome Discoverer. Data were analyzed using a label-free quantification method and the protein false discovery rate was set to 1%. To elucidate the molecular functions and classifications of significant proteins, the enrichment analysis was performed using Gene Ontology-based PANTHER classification system. SF samples were matched to human (*Homo sapiens*), while FCS samples were matched to the bovine (*Bos taurus*) databases.

Statistics

Statistical analyses were performed using GraphPad Prism (GraphPad Software) version 9.0.2. Shapiro–Wilk test assessed data normality. Two-way ANOVA tests with Bonferroni or Tukey's adjustment for multiple comparisons were used to assess significance in cartilage uptake and cellular studies respectively. *P*-values <0.05 were considered statistically significant and data are presented as mean values ± 95% CI unless otherwise indicated. Statistical and differential analyses for proteomic studies were performed in R (R Foundation for Statistical Computing), using LIMMA, DEP, and ComplexHeatmap R packages. To account for inconsistencies and skewness in the obtained data, the analysis was performed using the Mann Whitney Wilcoxon test followed by the Benjamini–Hochberg multiple hypothesis correction. Significance threshold was set for the adjusted *P*-values of <0.05 and ratio change of >1.5 fold.

Results

Material composition and characterization

To compare the effect of the SF protein corona formation and its influence on NP uptake into tissues and cells, three NP candidates with distinct surface chemistries were formulated. Products were confirmed by ^{1}H nuclear magnetic resonance spectroscopy (Fig. S1) and consisted of PAMAMs containing no PEG (NP_0), short PEG chains (NP_{350}), or long PEG chains (NP_{5000}) conjugated with a FITC fluorophore. The size assessment of the NPs by TEM and DLS confirmed the expected sizes (theoretical size of PAMAM $G5 = 5.4$ nm; Fig. 1(A) and (B)). NP_0 measured 7.2 ± 2.8 nm, NP_{350} measured 7.8 ± 2.5 nm, and as expected, NP_{5000} exhibited the largest hydrodynamic radius of 11.0 ± 4.4 nm. Similarities between NP_0 and NP_{350} were also seen in the zeta potential characteristics, where recorded values were $+17.0 \pm 1.78$ mV and $+16.0 \pm 1.95$ mV, respectively. NP_{5000} exhibited a lower value of $+4.0 \pm 2.57$ mV [Fig. 1(C)]. The similar FITC fluorescence profiles between all NPs

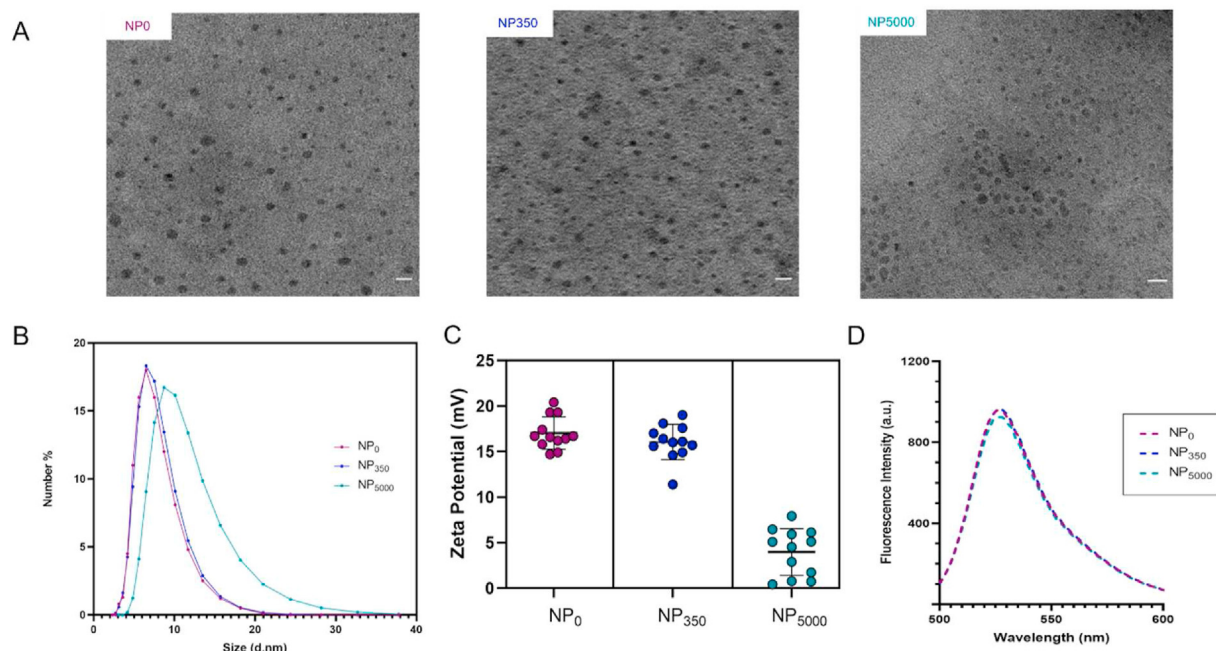**Fig. 1**   Osteoarthritis and Cartilage

PAMAM-PEG$_x$-FITC NP characterization (A) The sizes of the NPs were assessed with TEM in a 15 µM PBS suspension at pH = 6, scale bar = 10 nm (B, C) The hydrodynamic diameter of the particles was measured at 30 µM, neutral pH environment and the values were extracted based on the size distribution by volume, and zeta potential was quantified using DLS (D) Green fluorescence FITC signal was measured and quantified λ = ex. 483/14 nm, λ = em. 530/30 nm by a fluorescence spectrophotometer.

allowed fluorescence quantification to be used as a method for NP tracking in biological assays [Fig. 1 (D)].

Cytotoxicity of the NPs was evaluated on three different cell types due to their varied sensitivity: mouse fibroblast (L929 cells, based on FDA guidelines[16]), human chondrocyte (Tc28a2), and monocyte (U937) cell lines (Fig. S2). Cellular tolerance (defined as cell viability below 70% according to ISO 10993-5[16]) was observed at concentrations below 50 μM, thus, the concentration used in all biological assays was set to 30 μM.

Protein adsorption to NP surfaces naturally resulted in heterogeneous and increased NP sizes (data not shown) and a shift toward negative charges (Fig. S3 A–B). BCA protein quantification revealed the highest concentration of adhered protein from RA SF, followed by FCS and OA (Fig. S3 C). SF-derived coronas yielded zeta potentials ranging from -13.9 ± 1.4 mV (NP_{5000}) to -15.7 ± 1.6 mV (NP_0) for OA, and from -12.9 ± 1.2 mV (NP_{5000}) to -15.5 ± 1.2 mV (NP_0) for RA. Meanwhile, FCS condition ranged from -9.4 ± 4.1 mV (NP_0) to -10.5 ± 3.0 mV (NP_{5000}).

Cartilage uptake studies of hard protein corona-coated NPs

NP capacity to interact with cartilage tissue was assessed by quantifying the FITC signal over time. Reduced fluorescent signal in the media suggested that all NPs (NP_0, NP_{350}, NP_{5000}) were able to interact with the viable cartilage. All candidates subjected to PBS (no protein condition) displayed a significant uptake ($P < 0.0001$, 95% CI = 5.72–12.98; p = 0.0002, 95% CI = 3.48–11.18; p = 0.0017, 95% CI = 2.18–9.82) after 24 h [Fig. 2 (A)]. However, hard protein corona-decorated NPs displayed a difference depending on the protein source. NP_0 [Fig. 2 (B)] and NP_{350} [Fig. 2(C)] displayed a significant change in fluorescence only in FCS condition ($P = 0.0089$, 95% CI = 2.18–16.99; p = 0.0098, 95% CI = 1.73–14.20, respectively). NP_{5000} proved to be the most effective candidate as it displayed significant changes in fluorescence and subsequent uptake into cartilage in OA ($P = 0.0036$, 95% CI = 2.68–14.88) and FCS ($P = 0.0343$, 95% CI = 0.40–12.60) conditions. NP uptake and association with the cartilage tissue were further supported by fluorescent imaging. Prominent effects of the protein conditions were observed for NP_0 [Fig. 2 (F)], but not for the PEGylated NP_{350} and NP_{5000} (Fig. S4 A–B).

Particle uptake by cartilage associated cells

The influence of the biological identity of NPs was further evaluated in chondrocyte and monocyte lines, as well as RA and OA patient FLS cells. FITC uptake was measured using flow cytometry and all cells were incubated with NPs for 30 min or 10 h (Figure D). Additional time points were investigated in chondrocyte and monocyte cell lines (Fig. S5). We observed a higher cellular uptake under protein-free (PBS) conditions as compared to NPs subjected to protein adsorption (Fig. 3). Tc28a2 chondrocytes displayed NP uptake regardless of protein coronas (Fig. 3 A1-4), especially with the NP_{5000}. Interestingly, RA-derived FLS displayed a prominent difference for all NPs after 30 min under protein-free conditions, but especially for NP_{5000} (Fig. 3 D1). U937 monocytes took up NP_{5000} most efficiently after 10 h in both protein-free (Fig. 3 B1) and FCS conditions (Fig. 3(B)4). No selectivity was observed for any of the NPs in SF conditions (Fig. 3 B2-3).

Patient-derived primary OA FLS had no preference for NP uptake in protein-free conditions (Fig. 3C1), whereas NP_0 was taken up more effectively with an OA SF-derived protein corona (Fig. 3C2). The RA-derived protein corona only influenced the chondrocyte uptake after 10 h, while a 30-min incubation time of NP_0 was most efficient with FCS conditions (Fig. 3C4). RA patient-derived FLS displayed no distinguishable difference in uptake for any of the NPs in protein-rich conditions (Fig. 3 D2-4).

Characterization of hard protein corona-coated NPs

Gene ontology analysis of protein molecular function provided a general overview of OA, RA, and FCS condition differences illustrating functional similarities despite FCS proteins arising from a different animal species [Fig. 4(A)–(C)]. Proteins exhibiting binding or catalytic activity constituted a large part of the hard protein corona found on all NPs. Protein activity binding modulators such as C3, C4BPA, C5, ITIH1, ITIH2, ITIH4, SERPINA3, ARF4, HRG, GFA, HSPB1, and others composed the largest part of the differentially abundant proteins in SF [Fig. 4(D) and (E)], comprising of 26% and 18% of the total significant protein count in OA and RA, respectively. In contrast, the largest group of proteins in FCS samples were classified as protein modifying enzymes and included 25% of the significant proteins, followed by cytoskeletal proteins which comprised 17% of the total significant protein count [Fig. 4 (F)].

The most abundant proteins identified in the SF samples included albumin, lubricin, fibronectin, inflammation-associated proteins, and numerous apolipoproteins. The high abundance of components such as myeloperoxidase, complement proteins such as C1s, C3, C4a/b, C9, hemoglobin subunit beta, as well as the findings of various immunoglobulins confirmed the inflammatory state. ECM-associated proteins such as inter-alpha-trypsin inhibitor heavy chains, cartilage acidic protein 1, cartilage oligomeric matrix protein, and alpha-2-HS-glycoprotein were also detected. Additionally, we discovered other proteins which take part in various cellular processes and protein transport such as heparin cofactor 2, prothrombin, actin-binding gelsolin, histone components, and others.

Most abundant proteins found in FCS conditions correlated with some of the proteins found in the synovial patient samples. Similarities between the SF and FCS included albumin, complement factors, fibrinogen, inter-alpha-trypsin inhibitor heavy chains, and various apolipoproteins.

Differentially abundant proteins between OA and RA included COMP, ITIH1, ITIH2, and SIGLEC5. While these proteins were detected on the NP_{350} particle, abundance was not as prominent on the NP_{5000}. NP_0 showed a similar profile to NP_{5000} with high abundances seen in proteins involved in transport such as ARF4, ACAP1, RP2 [Fig. 5 (A)] in OA SF conditions. NPs with RA SF-derived coronas were prominent in EMC8, GYS2, H2BC3, TOLLIP [Fig. 5 (B)]. NPs with proteins from FCS showed distinct differential abundances for a variety of proteasome subunits [Fig. 5(C)], including multiple members of PSMB and PSMA families.

Discussion

The nature of the intrinsic biological environment is an important consideration that often is neglected in many drug delivery vehicle studies[17]. Our study addressed this issue by evaluating the influence of patient-derived SF protein coronas on three types of NPs and their ability to be taken up by cartilage tissue and joint-associated cells.

Aiming to preserve the cationic profile of the PAMAMs for electrostatically driven cartilage transport, a 2% surface PEGylation equipped NPs with distinct surface chemistries while maintaining the small size (<15 nm) needed for cartilage tissue penetration[13]. NP_{5000} characterized by the long chains of PEG proved to be the most tolerated in the cytotoxicity assessment, thus supporting the importance of PEGylation as a strategy for enhancing biocompatibility[18].
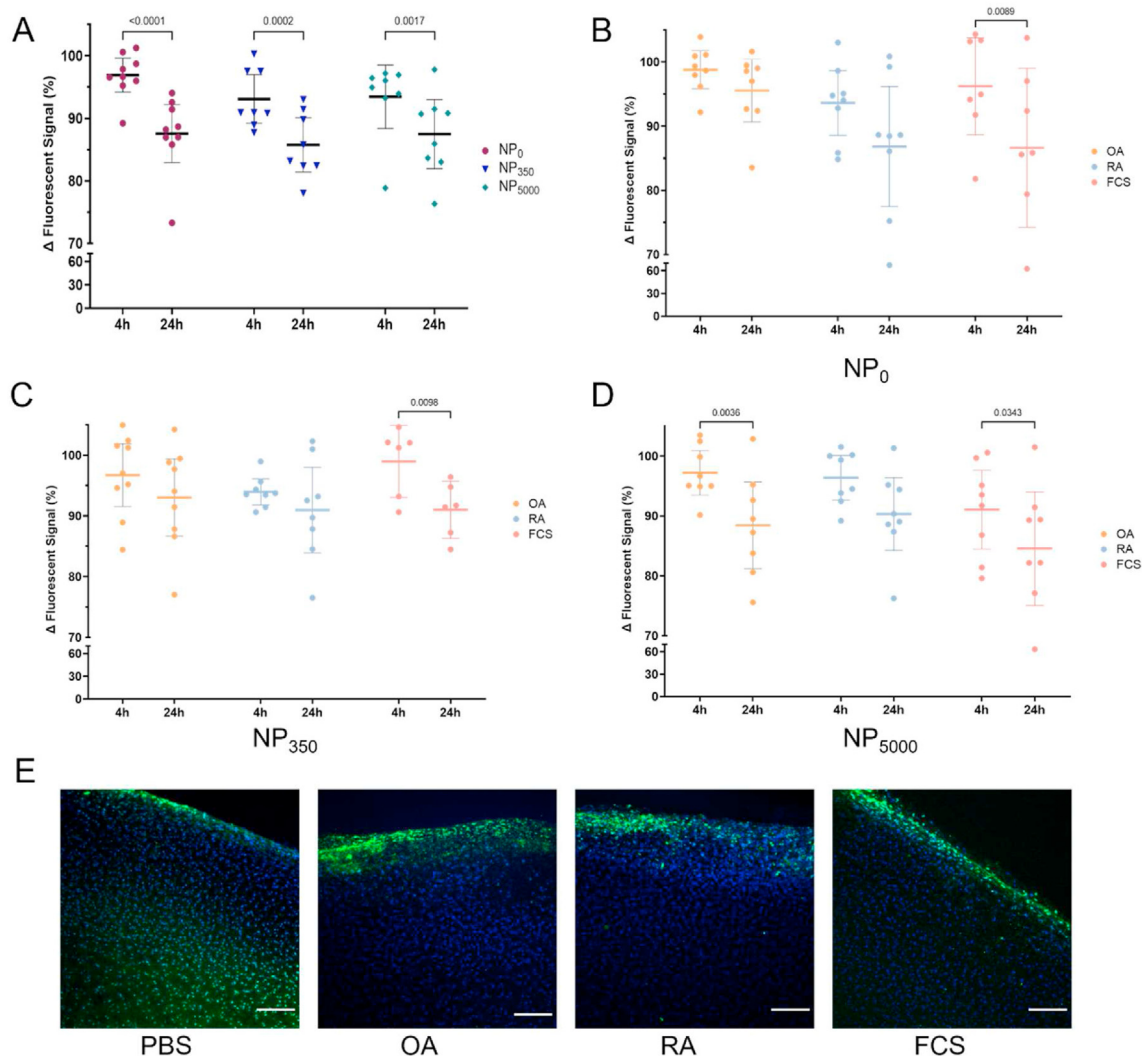
Fig. 2

Osteoarthritis and Cartilage

Investigation of NP uptake to the cartilage tissue explants (A) 30 μM of NPs were administered to cartilage explants and incubated for 4 h or 24 h. FITC signal was detected using a fluorescence spectrophotometer and NP uptake into the cartilage tissue was assessed after 4- or 24-h incubation and normalized to its correspondent pre-incubation signal. Each NP suspension was subjected to three different protein abundant conditions − OA = pooled OA patient synovial fluid (2f/2m); RA = pooled RA patient synovial fluid (4f/1m); FCS = fetal calf serum. The influence of the formed hard protein corona on cartilage uptake was compared for NP_0, NP_{350}, and NP_{5000}, respectively (B, C, D) (E) Representative confocal images of cartilage uptake of NP_0 particles after 24h. Nanoparticles appear as green due to FITC tag, while DAPI allows visualization of the chondrocytes in the tissue. Scale bar indicates 50 μm. Data are representative of 3 independent experiment repeats, $n = 4$–9. Error bars represent 95% CI, while the statistical significance was assessed using 2-way ANOVA with Bonferroni correction.

It is known that the composition behind protein corona formation is dictated by interpatient heterogeneity[8] and can further deviate depending on the "soft" (low affinity) and "hard" (high affinity) adhered protein layer[19]. Interestingly, we observed the highest protein concentration on NPs subjected to RA SF, followed by FCS, and OA SF, indicating differences based on the protein source and not the NP surface chemistry. Nevertheless, our PEGylation strategy did not inhibit protein adhesion to the NPs in general, resulting in particle size increase and reduced zeta potential, likely arising from the negatively charged proteins present in SF and serum[10]. As intra-articular NP drug delivery systems shift from

sustained-release to enhanced tissue penetration to target cartilage cells[20], considerations of protein corona effects will play a substantial role from pre-clinical development to success in the clinics and the emerging field of personalized medicine[21].

To evaluate the effect of protein adsorption on the uptake of our NPs, we utilized articular porcine cartilage explants as a model system. The thickness and structural similarities to human cartilage make them appropriate models for NP uptake since larger animal models are more relevant for mimicking cartilage pathologies such as OA[22]. All three NPs exhibited uptake into the cartilage over time. While no difference was observed under protein-free conditions,
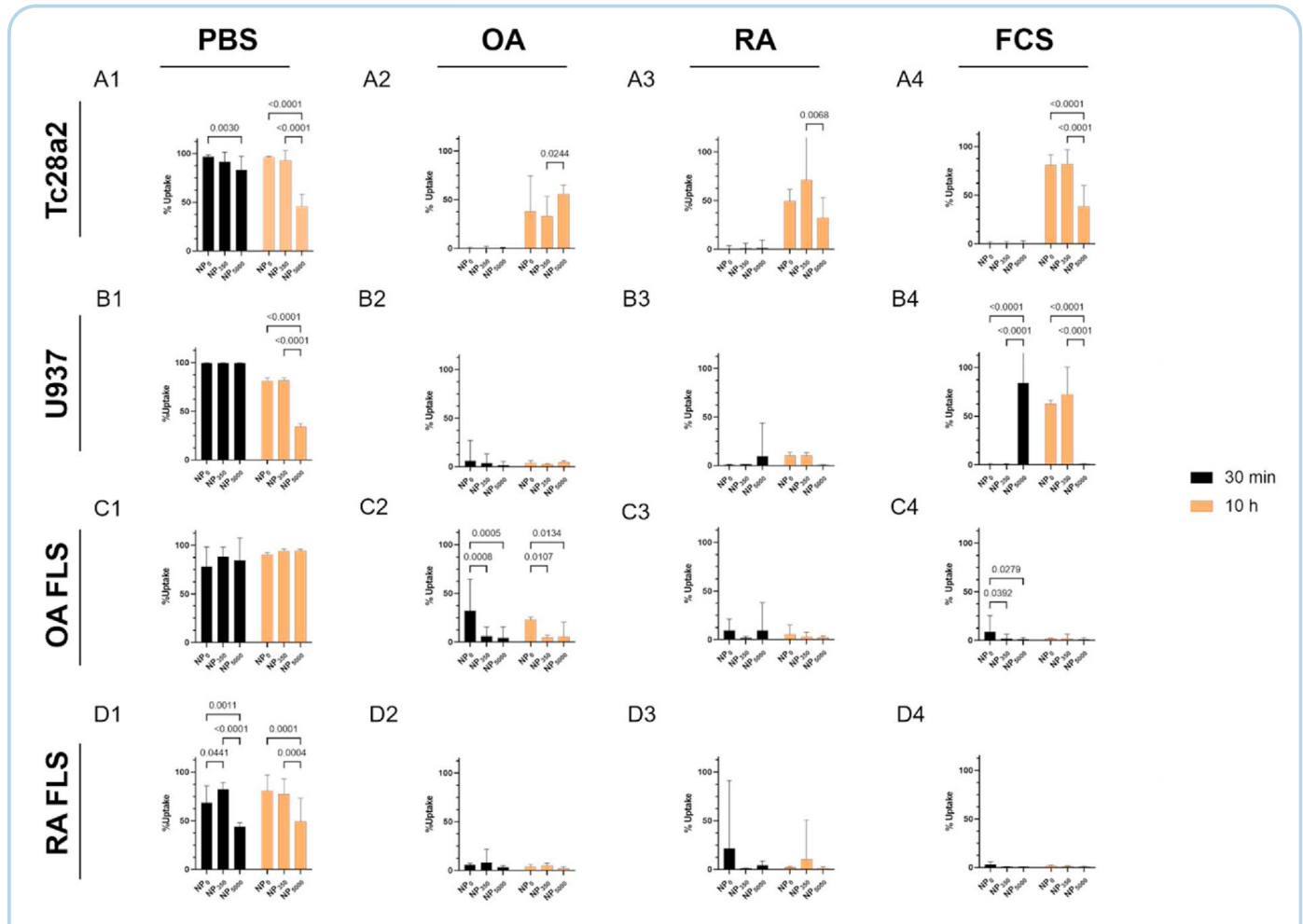
Fig. 3

Osteoarthritis and Cartilage

Assessment of NP uptake in Tc28a2 chondrocytes (A), U937 monocytes (B), OA FLS (C), and RA FLS (D) after 30 min and 10-h incubations. NPs were pre-incubated with either PBS (1), SFs from OA (2) or RA (3) patients, or FCS (4) for 1 h before the addition to the cells. FITC fluorescence of NPs was used as an indication of cellular uptake and represented as a % of the total cell count within the gate. Data were analyzed using 2-way ANOVA complimented with Tukey's test to assess the significance. P-values above 0.05 were regarded as significant, error bars represent 95% CI.

protein coronas interfered with the uptake of NPs into the tissue. All NPs displayed a significant uptake in FCS conditions. Interestingly, NP_{5000} also displayed a prominent uptake when subjected to OA SF conditions, suggesting the potential as a drug delivery vehicle in OA. The effect of PEGylation has been reported to aid in extracellular barrier transport in tissues such as brain and mucosal tissues[23], thus the longer PEG chains of the NP_{5000} could further advance the NP transport in cartilage ECM.

Further, the examined protein conditions affected NP interactions with the cartilage surface. Protein-free NPs reached deeper into the tissue compared to their NP-protein complex counterparts, as the complexes mainly localized to the superficial zone of the cartilage. Interestingly, no difference could be noted for the different PEGylated NPs, confirming that the biological identity of NPs plays a more prominent role in their interactions with the cartilage. Yet, it is important to note that the interactions between the human SF and porcine-derived cartilage may contain species-

dependent differences, requiring additional considerations for translational extrapolation.

For treatments aiming to target joints, it is important to not only consider the tissue barrier, but also the intended cellular target. Cellular uptake was studied in both chondrocyte and monocyte cell lines, as well as patient-derived OA and RA FLS cells. These were chosen to reflect the key players in the joint that would determine the outcomes of administered therapies[24–26]. Protein-free NPs exhibited a higher uptake when compared to NPs with protein coronas. These results contrast the tissue uptake studies as the NP uptake was visualized for all NPs regardless of surface modifications or protein conditions. We also noted that the usage of common lab reagents such as FCS or cell lines may lead to an overestimation of NP uptake. Interestingly, we observed different uptake profiles between OA and RA FLS cells under protein-free conditions, as OA FLS uptake was similar for all three NP types. In contrast, RA FLS were prominently less susceptible to NP_{5000}.
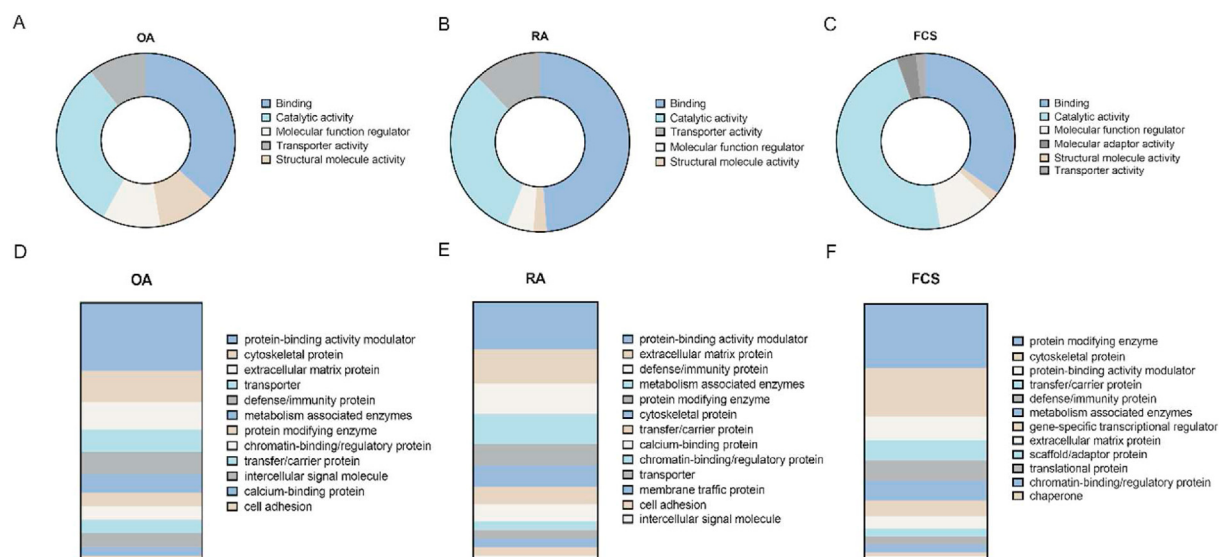
Fig. 4

Osteoarthritis and Cartilage

Pathway enrichment analysis for the differential protein abundances on the coronas detected in the panel of NP$_0$, NP$_{350}$, NP$_{5000}$ (A, B, C) PANTHER based analysis revealed molecular function of the identified proteins in human patient OA synovial fluid, human patient RA synovial fluid), and bovine fetal calf serum (FCS) samples, respectively (D, E, F) To further compare the difference between the detected proteins on the NP coronas, protein classification was also elucidated for the OA, RA, and FCS samples respectively using the same analysis comparison.
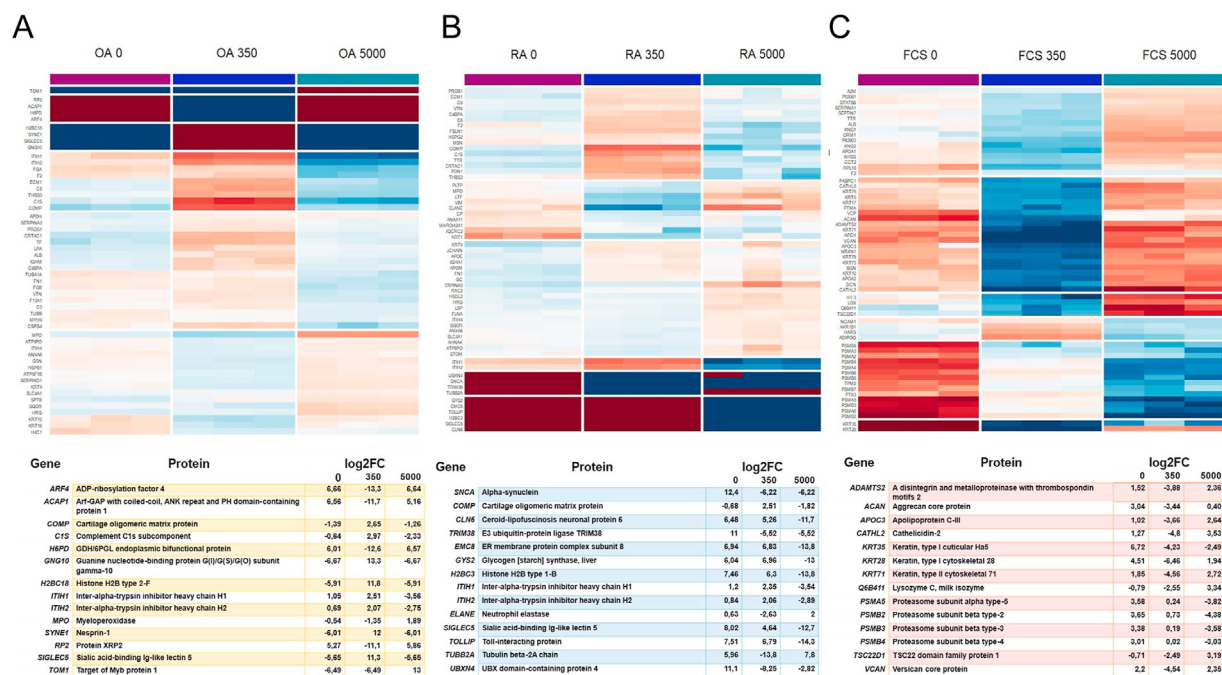

Fig. 5

Osteoarthritis and Cartilage

(A, B, C) Heat maps of the differentially expressed significant proteins associated with individual protein coronas on NP$_0$, NP$_{350}$, and NP$_{5000}$ exposed to late-stage OA synovial fluid (52) (A, B, C), RA synovial fluid (58), or commercially available FCS (59) respectively. The red and blue color scheme indicates high and low abundance of LFQ intensities (FDR = 1%) represented as log2FC. The tables below summarize the top 14 differentially expressed proteins among the NP groups.

Similarly, the chondrocyte and monocyte cell lines also exhibited significantly lower cellular uptake of NP_{5000} compared to NP_0 and NP_{350}. The lower uptake of NP_{5000} could be attributed to the PEGylation effect, as PEG chain length has been shown to decrease cellular interactions[27]. As many drugs aim to alter the ECM-producing chondrocytes, PEGylation could facilitate the transport of NPs through the ECM yet result in reduced cellular uptake. Future studies should investigate the ability of NPs to reach the native tissue-residing chondrocytes and their intracellular localization, as this may have implications on cellular responses irrespective of NP cargo.

Finally, to investigate if the observed uptake differences could be attributed to a specific protein and its function, we used a quantitative proteomics approach to assess individual protein corona profiles. In total, we identified 52, 58, and 59 statistically different abundant proteins among the NPs for OA, RA, and FCS conditions, respectively. Patient SFs were characterized by a differential expression of proteins such as TOM1 in OA, and TOLLIP in RA. Literature has recently linked TOM1 protein with endosomal transport, impaired autophagy, and immune response, thus likely contributing to the pathological mechanisms in both RA and OA[28,29]. TOM1, the most abundant protein on NP_{5000}, represents an interesting candidate that could direct NP uptake, as it is responsible for recruiting clathrin and driving endosomal cellular uptake. This could explain the significance of cartilage explant uptake for both OA and RA[30], as TOLLIP has been reported to associate with TOM1, thus together they may direct NP uptake into cells via endocytic pathways[30,31]. The differential adherence of TOM1, TOLLIP, and proteins alike might help to explain the differences seen in the biological uptake studies. Additionally, we were able to demonstrate the specificity of certain proteins such as COMP and ITIH1/2 to NP_{350} in both RA and OA conditions, suggesting that the surface chemistry of the NPs affects protein corona composition.

Additional studies in vivo and the utilization of microfluidic devices or bioreactors would allow for a more accurate representation of the joint in the future. As the synovial environment is highly dynamic, a major drawback of these studies includes SF turnover that may influence the diffusion and clearance rate of drug delivery agents[32]. Enhanced stability characterization of NPs subjected to protein-abundant conditions would allow the distinction between the NP aggregation profiles when compared to the preservation of the NP biological identity. Yet, to fully understand the impact of the protein corona formation on nanocarriers, distinct and robust characterization techniques are required and remain to be established in order to enhance the reproducibility, allow the comparisons among different NP systems, and enhance the translational capacity in nanomedicine[33].

To conclude, our study demonstrates the influence of protein corona interactions with small cationic NPs. It demonstrates how the biological identity of NPs dictates cartilage tissue and cellular uptake, and alludes to the role of PEGylation for ECM and cell surface interactions. While the question of how to optimally account for protein corona effects across the pre-clinical to clinical spectrum, these results encourage a continued outlook for biological identity characterization and studies mimicking the native cartilage tissue environment to enhance the development of nanomedicines for arthritis.

Author contributions

UvM and A.S designed the studies. UvM synthesized the polymers, conducted the *in vitro* and ex vivo studies and performed analysis. G.E conducted the NMR and fluorescent studies and analysis. T.S and L.R performed *in vitro* assays and analysis. A.K.H.E provided patient samples and helped with data interpretation. UvM and A.S wrote the manuscript with contributions from all authors, who also approved the final version.

Conflict of interest

Authors declare no competing interests.

Acknowledgements

Supplementary data

Supplementary data to this article can be found online at https://doi.org/10.1016/j.joca.2022.07.002.

References

1. Bajpayee AG, Grodzinsky AJ. Cartilage-targeting drug delivery: can electrostatic interactions help? Nat Rev Rheumatol 2017;13(3):183–93, https://doi.org/10.1038/nrrheum.2016.210.
2. Bajpayee AG, Scheu M, Grodzinsky AJ, Porter RM. Electrostatic interactions enable rapid penetration, enhanced uptake and retention of intra-articular injected avidin in rat knee joints. J Orthop Res 2014;32(8):1044–51, https://doi.org/10.1002/jor.22630.
3. Jin GZ. Current nanoparticle-based technologies for osteoarthritis therapy. Nanomaterials 2020;10(12):1–20, https://doi.org/10.3390/NANO10122368.
4. Glyn-Jones S, Palmer AJR, Agricola R, Price AJ, Vincent TL, Weinans H, *et al.* Osteoarthritis. Lancet 2015;386(9991):376–87, https://doi.org/10.1016/S0140-6736(14)60802-3.
5. Lundqvist M, Cedervall T. Three decades of research about the corona around nanoparticles: lessons learned and where to go now. Small 2020;16(46), 2000892, https://doi.org/10.1002/smll.202000892.
6. Madathiparambil Visalakshan R, González García LE, Benzigar MR, Ghazaryan A, Simon J, Mierczynska-Vasilev A, *et al.* The influence of nanoparticle shape on protein corona formation. Small 2020;16(25), 2000285, https://doi.org/10.1002/smll.202000285.
7. Mirshafiee V, Kim R, Mahmoudi M, Kraft ML. The importance of selecting a proper biological milieu for protein corona analysis in vitro: human plasma versus human serum. Int J Biochem Cell Biol 2016;75:188–95, https://doi.org/10.1016/j.biocel.2015.11.019.
8. Ju Y, Kelly HG, Dagley LF, Reynaldi A, Schlub TE, Spall SK, *et al.* Person-specific biomolecular coronas modulate nanoparticle interactions with immune cells in human blood. ACS Nano 2020;14(11):15723–37, https://doi.org/10.1021/acsnano.0c06679.
9. Morgen M, Tung D, Boras B, Miller W, Malfait AM, Tortorella M. Nanoparticles for improved local retention after intra-articular injection into the knee joint. Pharm Res (N Y) 2013;30(1):257–68, https://doi.org/10.1007/S11095-012-0870-X.
10. Brown S, Pistiner J, Adjei IM, Sharma B. Nanoparticle properties for delivery to cartilage: the implications of disease state, synovial fluid, and off-target uptake. Mol Pharm 2017;16(2):

469—79, https://doi.org/10.1021/ACS.MOLPHARMACEUT.7B00484.

11. Zhang M, Zhu J, Zheng Y, Guo R, Wang S, Mignani S, *et al.* Doxorubicin-conjugated PAMAM dendrimers for PH-responsive drug release and folic acid-targeted cancer therapy. Pharmaceutics 2018;10(3), https://doi.org/10.3390/PHARMACEUTICS10030162.

12. Abedi-Gaballu F, Dehghan G, Ghaffari M, Yekta R, Abbaspour-Ravasjani S, Baradaran B, *et al.* PAMAM dendrimers as efficient drug and Gene delivery nanosystems for cancer therapy. Elsevier Ltd September. Appl Mater Today 2018;1:177—90, https://doi.org/10.1016/j.apmt.2018.05.002.

13. Geiger BC, Wang S, Padera RF, Grodzinsky AJ, Hammond PT. Cartilage-penetrating nanocarriers improve delivery and efficacy of growth factor treatment of osteoarthritis. Sci Transl Med 2018;10(469):1—13, https://doi.org/10.1126/scitranslmed.aat8800.

14. Åkesson A, Cárdenas M, Elia G, Monopoli MP, Dawson KA. The protein corona of dendrimers: PAMAM binds and activates complement proteins in human plasma in a generation dependent manner. RSC Adv 2012;2(30):11245—8, https://doi.org/10.1039/C2RA21866F.

15. Zhao D, Xu JQ, Yi XQ, Zhang Q, Cheng SX, Zhuo RX, *et al.* PH-activated targeting drug delivery system based on the selective binding of phenylboronic acid. ACS Appl Mater Interfaces 2016;8(23):14845—54, https://doi.org/10.1021/ACSAMI.6B04737/SUPPL_FILE/AM6B04737_SI_001.PDF.

16. ISO - ISO 10993-5:2009 - Biological evaluation of medical devices — Part 5: Tests for in vitro cytotoxicity https://www.iso.org/standard/36406.html (accessed Nov 2, 2021).

17. Berrecoso G, Crecente-Campo J, Alonso MJ. Unveiling the pitfalls of the protein corona of polymeric drug nanocarriers. Drug Deliv. Transl. Res. 2020;10(3):730—50, https://doi.org/10.1007/s13346-020-00745-0.

18. Partikel K, Korte R, Stein NC, Mulac D, Herrmann FC, Humpf HU, *et al.* Effect of nanoparticle size and PEGylation on the protein corona of PLGA nanoparticles. Eur J Pharm Biopharm 2019;141:70—80, https://doi.org/10.1016/J.EJPB.2019.05.006.

19. García-Álvarez R, Vallet-Regí M. Hard and soft protein corona of nanomaterials: analysis and relevance. Nanomaterials 2021;11(4), https://doi.org/10.3390/NANO11040888.

20. Huang H, Lou Z, Zheng S, Wu J, Yao Q, Chen R, *et al.* Intra-articular drug delivery systems for osteoarthritis therapy: shifting from sustained release to enhancing penetration into cartilage. Drug Deliv 2022;29(1):767—91, https://doi.org/10.1080/10717544.2022.2048130.

21. Mitchell MJ, Billingsley MM, Haley RM, Wechsler ME, Peppas NA, Langer R. Engineering precision nanoparticles for drug delivery. Nat Rev Drug Discov 2020;20(2):101—24, https://doi.org/10.1038/s41573-020-0090-8. 2020 202.

22. Kuyinu EL, Narayanan G, Nair LS, Laurencin CT. Animal models of osteoarthritis: classification, update, and measurement of outcomes. J Orthop Surg Res 2016;11(1), https://doi.org/10.1186/S13018-016-0346-5.

23. Labouta HI, Gomez-Garcia MJ, Sarsons CD, Nguyen T, Kennard J, Ngo W, *et al.* Surface-grafted polyethylene glycol conformation impacts the transport of PEG-functionalized liposomes through a tumour extracellular matrix model. RSC Adv 2018;8(14):7697—708, https://doi.org/10.1039/c7ra13438j.

24. McInnes IB, Schett G. Pathogenetic insights from the treatment of rheumatoid arthritis. Lancet 2017;389(10086):2328—37, https://doi.org/10.1016/S0140-6736(17)31472-1.

25. Bosch MHJ van den. Osteoarthritis year in review 2020: biology. Osteoarthritis Cartilage 2021;29(2):143—50, https://doi.org/10.1016/J.JOCA.2020.10.006.

26. Moradi B, Rosshirt N, Tripel E, Kirsch J, Barié A, Zeifang F, *et al.* Unicompartmental and bicompartmental knee osteoarthritis show different patterns of mononuclear cell infiltration and cytokine release in the affected joints. Clin Exp Immunol 2015;180(1):143—54, https://doi.org/10.1111/cei.12486.

27. Deshpande MC, Davies MC, Garnett MC, Williams PM, Armitage D, Bailey L, *et al.* The effect of poly(ethylene glycol) molecular architecture on cellular interaction and uptake of DNA complexes. J Contr Release 2004;97(1):143—56, https://doi.org/10.1016/J.JCONREL.2004.02.019.

28. Roach TG, Lång HKM, Xiong W, Ryhänen SJ, Capelluto DGS. Protein trafficking or cell signaling: a dilemma for the adaptor protein TOM1. Front Cell Dev Biol 2021:408, https://doi.org/10.3389/FCELL.2021.643769. 0.

29. Keskitalo S, Haapaniemi EM, Glumoff V, Liu X, Lehtinen V, Fogarty C, *et al.* Dominant TOM1 mutation associated with combined immunodeficiency and autoimmune disease. npj Genomic Med 2019;4(1):1—7, https://doi.org/10.1038/s41525-019-0088-5. 2019 41.

30. Katoh Y, Imakagura H, Futatsumori M, Nakayama K. Recruitment of clathrin onto endosomes by the tom1-tollip complex. Biochem Biophys Res Commun 2006;341(1):143—9, https://doi.org/10.1016/j.bbrc.2005.12.156.

31. Xiao S, Brannon MK, Zhao X, Fread KI, Ellena JF, Bushweller JH, *et al.* Tom1 modulates binding of tollip to phosphatidylinositol 3-phosphate via a coupled folding and binding mechanism. Structure 2015;23(10):1910—20, https://doi.org/10.1016/j.str.2015.07.017.

32. Mekheimer KS, Abo-Elkhair RE, Abdelsalam SI, Ali KK, Moawad AMA. Biomedical simulations of nanoparticles drug delivery to blood hemodynamics in diseased organs: synovitis problem. Int Commun Heat Mass Tran 2022;130, 105756, https://doi.org/10.1016/j.icheatmasstransfer.2021.105756. December 2021.

33. Mahmoudi M. The need for improved methodology in protein corona analysis. Nat Commun 2022;13(1):1—4, https://doi.org/10.1038/s41467-021-27643-4. 131 2022.